

The Potential of Convolutional Neural Networks for Cancer Detection

Hossein Molaieian, Kaveh Karamjani, Sina Teimouri, Saeed Roshani, and Sobhan Roshani

Department of Computer Engineering, Islamic Azad University,
Kermanshah 6718997551, Iran

ABSTRACT:

Early detection of cancer is critical in improving treatment outcomes and increasing survival rates, particularly for common cancers such as lung, breast and prostate which collectively contribute to a significant global mortality burden. With advancements in imaging technologies and data processing, Convolutional Neural Networks (CNNs) have emerged as a powerful tool for analyzing and classifying medical images, enabling more precise cancer detection. This paper provides a comprehensive review of recent studies leveraging CNN models for detecting ten different types of cancer. Each study employs distinct CNN architectures to identify patterns associated with these cancers, utilizing diverse datasets. Key differences and strengths of these architectures are meticulously compared and analyzed, highlighting their efficacy in improving early detection. Beyond reviewing the performance and limitations of CNN-based cancer detection methods, this study explores the feasibility of integrating CNNs into clinical settings as an early detection tool, potentially complementing or replacing traditional methods. Despite significant progress, challenges remain, including data diversity, result interpretation, and ethical considerations. By identifying the best-performing CNN architectures and providing a comparative analysis, this study aims to contribute a comprehensive perspective on the application of CNNs in cancer detection and their role in advancing diagnostic capabilities in healthcare.

Index Terms—Cancer Detection, Convolutional Neural Networks (CNN), Machine Learning, Pattern Recognition.

I. INTRODUCTION

Cancer is one of the most complex and deadly diseases of the present century, and due to its increasing prevalence, it has become a global crisis. This disease is characterized by the uncontrolled growth of cells, which can spread to other parts of the body, leading to disability and death. The exact causes of cancer are highly diverse and are a combination of genetic, environmental, and lifestyle factors.

Cancer manifests in various forms throughout the body, with each type having its own distinct characteristics, symptoms, and risk factors. In this study, we focus on some of the most common types of cancer, including prostate cancer, blood cancers (leukemia and lymphoma), bladder cancer, skin cancer (melanoma and non-melanoma), colorectal cancer, liver cancer, breast cancer, ovarian cancer, thyroid cancer, and lung cancer. These cancers are of particular significance due to their high prevalence and considerable impact on public health.¹²

Global data indicate that the cancer burden is increasing annually. Several factors contribute to the rising prevalence of cancer, including increased life expectancy, lifestyle changes (such as poor diet, lack of physical activity, smoking), environmental factors (air pollution, radiation), and genetic factors.¹²

Early detection of cancer is the key to increasing the chances of recovery and reducing mortality associated with this disease. In the early stages, many cancers do not present obvious symptoms and may be detected incidentally during routine check-ups. With early detection, more effective treatment with fewer side effects becomes possible. imaging techniques play a crucial role in cancer diagnosis. These methods help doctors determine the size, shape, and location of tumors, and also assist in evaluating the spread of the disease.

Some of the most important imaging methods include radiography, which uses X-rays to create images of bones and soft tissues; ultrasound, which uses high-frequency sound waves to create images of internal organs; CT scan, which utilizes X-rays and a computer to create detailed cross-sectional images of the body; MRI, which employs magnetic fields and radio waves to generate highly accurate images of soft tissues; and PET scan, which uses a radioactive substance to create images of the metabolic activity of cells. These imaging techniques are essential in helping doctors identify and assess cancerous growths, their size, and how far the disease has spread.³

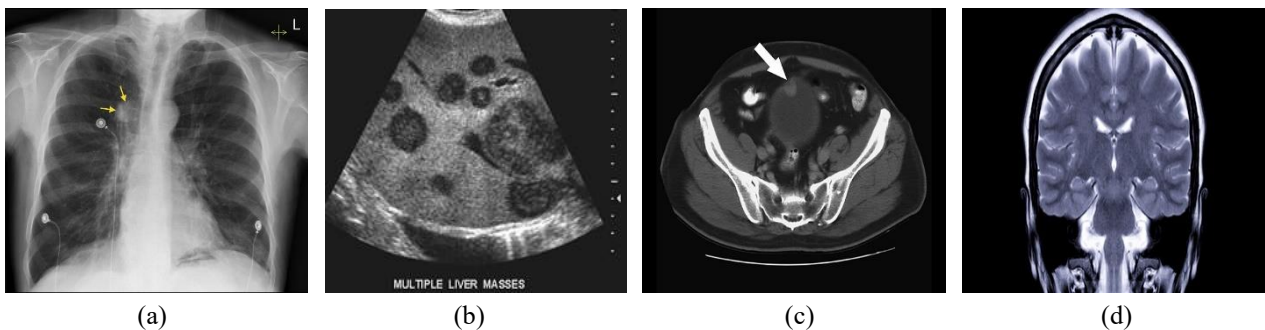
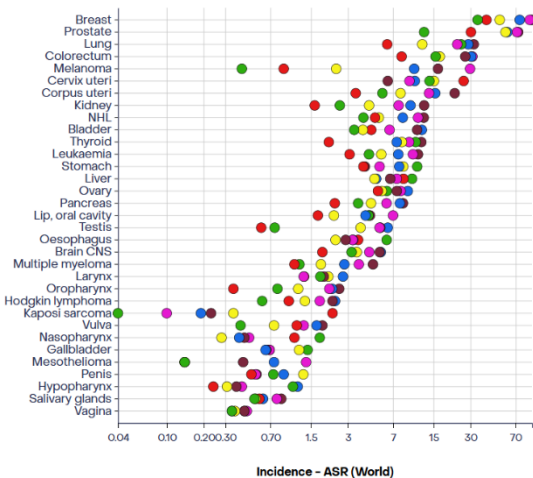


Fig1. Here are some examples of imaging techniques used for cancer diagnosis, with the labels assigned to each image: (a) Radiography, (b) Ultrasound, (c) CT scan, and (d) MRI.

In Table 1, a brief overview of the ten most common types of cancer is provided, selected due to their high prevalence and significant impact on public health.

Cancer Type	Annual Incidence Rate	Annual Mortality Rate	Annual Growth Rate (%)	Description
Prostate ⁴	1.4M	375,000	2.0%	One of the most common cancers in men, which develops in the prostate gland and grows slowly
Blood ²	476,000	311,000	1.5%	A type of cancer that usually begins in the blood cells and bone marrow, leading to an increase in abnormal blood cells.
Bladder ⁵	573,000	213,000	2.2%	Bladder cancer most often develops in the inner lining of the bladder and is more common in men.
Skin ²	325,000	57,000	3.0%	A type of cancer that begins in the melanin-producing cells of the skin and can spread to other parts of the body.
Colorectal ⁶	1.9M	935,000	1.8%	A type of cancer that begins in the melanin-producing cells of the skin and can spread to other parts of the body.
Liver ⁷	900,000	830,000	2.5%	Liver cancer often develops as a result of hepatitis or other liver damage and progresses rapidly.
Breast ⁸	2.3M	685,000	2.6%	The most common cancer among women, which begins in the cells of the milk glands or ducts of the breast.
Ovarian ⁹	313,000	207,000	1.4%	A type of cancer that begins in the ovaries and is often diagnosed at an advanced stage.
Thyroid ²	587,000	43,000	2.0%	A cancer that occurs in the thyroid gland, is more common in women, and is often treatable with surgery.
Lung ¹⁰	2.2M	1.8M	1.9%	One of the deadliest cancers, which develops in the lungs and is primarily caused by tobacco use.

Table 1. This table provides an overview of different types of cancer, including a brief description of each type, along with the number of annual deaths and new cases reported for each cancer type. These statistics highlight the significance and impact of these cancers on global health.



(Image 1)

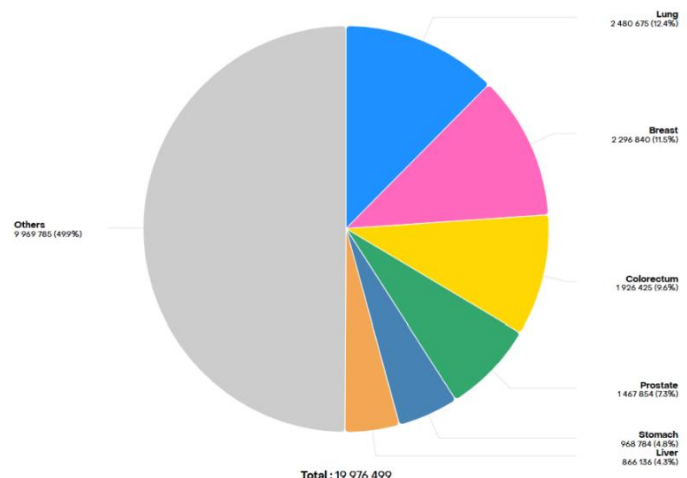


(Image 2)

Fig2. Image 1 illustrating the global age-standardized incidence rates (ASR) of various cancer types, highlighting disparities across cancer forms and regions and Image 2 showing the global distribution of cancer cases by type, with lung, breast, and colorectal cancers accounting for the largest shares.

CNN (Convolutional Neural Networks):

CNNs are among the most important and widely used artificial intelligence models in the field of image processing and pattern recognition. CNNs are particularly effective for identifying and classifying images, and they have found numerous applications in disease diagnosis, especially cancer detection. Below, a comprehensive explanation of the structure and functionality of these networks, as well as their role in cancer diagnosis, is provided.

A CNN is a type of artificial neural network specifically designed for analyzing visual data. CNNs are structured in a way that allows them to automatically identify the significant features of images and utilize these features for classification and recognition tasks. The structure of a CNN consists of several layers that progressively identify more complex features of an image. The main layers in a CNN include convolutional layers, pooling layers, and fully connected layers.¹¹

Convolutional Layer: This layer serves as the core of the Convolutional Neural Network (CNN), responsible for extracting features from the input image. It operates by sliding a filter over the image, detecting specific patterns, and extracting features such as edges, lines, and textures. Essentially, this layer analyzes neighboring pixels to extract structural information about the image.¹¹

Pooling Layer: Positioned after the convolutional layer, the pooling layer reduces the image's dimensionality. By decreasing the image size, the amount of computational work required by the network is reduced, leading to improved efficiency and performance. The most commonly used pooling technique is Max Pooling, which selects the maximum value from each small section of the image.¹¹

Fully Connected Layer: These final layers gather and classify the extracted data from the previous layers. At this stage, the CNN assigns the information to specific categories, such as different types of cancers or anomalies, enabling the model to make final predictions or decisions.¹¹

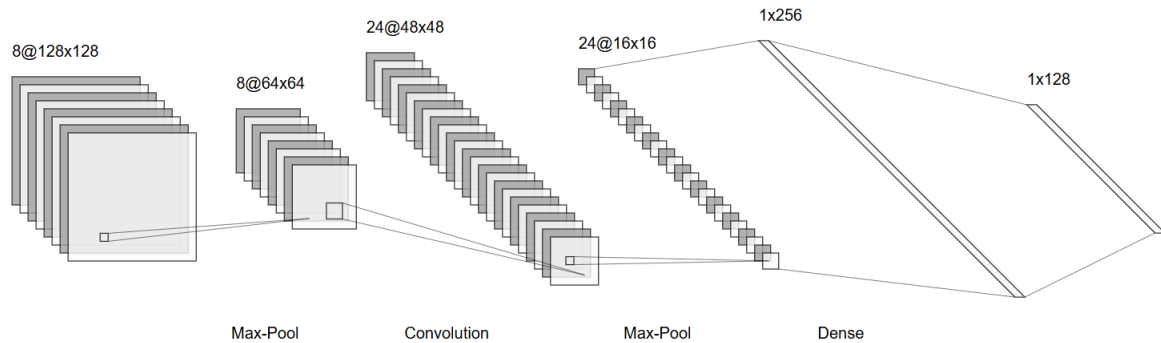


Fig3. This image illustrates the architecture of a Convolutional Neural Network (CNN), consisting of convolutional layers, max-pooling layers, and dense (fully connected) layers. Each layer sequentially extracts more complex features from the image data and ultimately uses them for classification.

Deep neural networks, including CNNs, are closely intertwined with the field of mathematics. Mathematics is the fundamental building block in the structure and functioning of these networks. One of the key reasons behind the power of neural networks is the use of complex mathematical equations and formulas to extract features, learn patterns, and make predictions. In other words, the entire learning process in neural networks is based on mathematical computations, which help the network analyze the input data and reach the desired outcomes.

Differentiation and optimization are other essential mathematical concepts in neural networks. To train the network and minimize errors, methods such as Gradient Descent are used. In this approach, differentiation is employed to find the minimum of the error function, enabling the network to achieve optimal performance. The error function or loss function is a metric that determines the network's prediction accuracy, and optimization algorithms work to minimize this error function.

In CNNs, formulas play a crucial role in the learning process. The error function measures the difference between the predicted output and the actual value. The weighted function determines the influence of each feature on the decision-making process, based on weights. Convolution operations, through filters, extract essential features from images. Meanwhile, gradient descent updates the weights to minimize the cost function, optimizing the model's performance. Together, these formulas enable the learning process and help the network improve its accuracy.¹¹

Weighted Sum and Bias:

In each neuron of a neural network, inputs are transferred to the neuron with specific weight values. This formula is as follows:

$$z = w_1x_1 + w_2x_2 + \dots + w_nx_n + b$$

(x) the input values are denoted by.

(w) represents the weights corresponding to each input.

(b) is the bias (a constant value) that helps the model have more flexibility.

Convolution in CNNs:

Convolution operation is used to combine features and extract local patterns from the image, and its formula is as follows:

$$S(i, j) = (I * K)(i, j) = \sum_m \sum_n I(i + m, j + n) \cdot K(m, n)$$

(I) is the input image matrix.

(K) is the kernel or filter matrix.

(S(i, j)) is the output value at the point ((i, j)).

Loss Function:

Error Function or Loss Function is used to evaluate the mistakes made by the model in its individual predictions. This function indicates how far the model's prediction is from the actual prediction. In simpler terms, when the model makes a prediction, the loss function tells how much the model's prediction deviates from reality. It helps the model understand where it went wrong and what adjustments need to be made.¹²

- For example, in a cancer detection model:

- If the model predicts that there is no cancer, but cancer is actually present, the loss function assigns a large value, indicating a significant mistake.

- If the model predicts that there is cancer and cancer is indeed present, the error is small.

Goal: The main objective in machine learning is to minimize this error, meaning the model should make accurate predictions.

The formula for the loss function for a single sample in binary problems (like cancer detection):

$$Loss = -[y \cdot \log(\hat{y}) + (1 - y) \cdot \log(1 - \hat{y})]$$

The true label is (y) (where 1 indicates the presence of cancer and 0 indicates its absence).

(\hat{y}) is the model's prediction (the predicted probability of cancer, a value between 0 and 1).

Cost Function:

Cost Function is a function that calculates the overall error of the model for all data (e.g., all images), as the name suggests.¹²

- The cost function provides the mean or sum of all the model's errors for all samples. It tells us how accurate the model is overall. If the cost function is high, it means the model has a lot of mistakes in its predictions.

Goal: The goal is to minimize the cost function so that the model can achieve higher accuracy and perform better in tasks like cancer detection or any other application. The formula for the cost function (which is the average of the error function for all samples):

$$Cost = \frac{1}{N} \sum_{i=1}^1 Loss_i$$

The number of samples (e.g., the number of images)

($Loss_i$) is the error for each individual sample.

Gradient Descent:

Gradient Descent is an optimization algorithm used to minimize the cost function and improve the model's accuracy. This algorithm helps the model find the best weights and biases so that the cost function achieves its lowest possible value.¹³

- Imagine the cost function as a curve. Gradient descent helps the model move from a high point on the cost function curve towards the lowest point.
- Gradient descent gradually updates the weights and biases to improve the model's performance in predictions.

How it works:

1. Calculate the gradients: First, the changes in the cost function with respect to the weights and biases (called parameters) are computed. These changes (gradients) indicate how much the weights and biases should change in order to reduce the cost function.
2. Update the weights and biases: Next, the weights and biases are updated using the gradients.
3. Repeat the process: This process is repeated until the cost function is minimized.

Weight and bias update formula in gradient descent:

$$w = w - \alpha \cdot \frac{\partial J(w, b)}{\partial w}$$

$$b = b - \alpha \cdot \frac{\partial J(w, b)}{\partial b}$$

(α) is the learning rate (a number that determines how large the weight updates should be).

Kernels in CNNs:

Kernels (or filters) are essential tools in CNNs that allow the network to detect and extract various patterns from images. Each kernel is a small matrix (e.g., 3×3 or 5×5) that moves across the image, performing a convolution¹⁴ operation (element-wise multiplication followed by summation) to extract specific features.

When a kernel is applied to an image, the result of the element-wise multiplication and summation (known as the convolution sum) becomes a single point in the feature map. This process is repeated across the entire image to extract patterns such as edges, textures, and other visual characteristics.

Applications of Kernels in Feature Extraction:

- Edge Detection: Edge-detection kernels, such as Sobel and Scharr filters, highlight sharp changes in brightness, capturing object boundaries and edges.
- Texture Recognition: Certain kernels are designed to detect complex textures, such as skin, fabric, or natural patterns like wood or stone.
- Line and Repetitive Pattern Detection: Kernels that focus on vertical, horizontal, or diagonal lines enable the network to recognize repeating patterns or geometric structures, such as those found in buildings.
- Brightness Adjustment and Bright Object Detection: Specific kernels help adjust brightness levels or identify bright regions and objects within an image.

At each convolutional layer, kernels extract features, enabling the network to perform deeper analysis and improving its accuracy in and classification tasks.



Fig4. This image illustrates the Max Pooling process in neural networks. A 4×4 input matrix is processed using a 2×2 filter with a stride of 2. For each 2×2 block, the maximum value is selected, resulting in a 2×2 output matrix. This operation helps reduce dimensionality while retaining important features of the data.

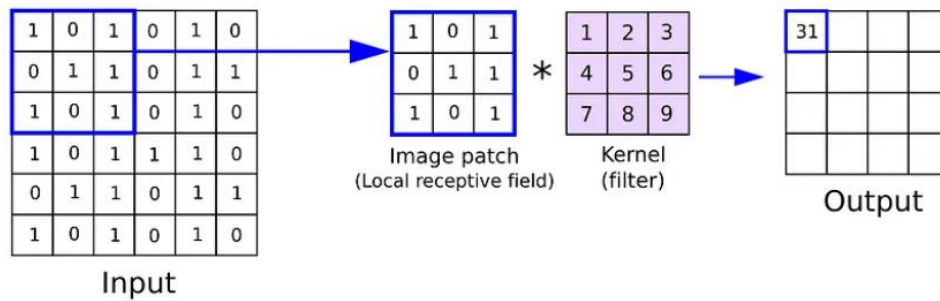


Fig5. This image illustrates the convolution process in neural networks. A small region of the input matrix (*Image Patch*) is selected and multiplied element-wise with a kernel (*filter*). The resulting products are summed up, and a single value is stored in the output matrix. This operation extracts important features and helps reduce the input dimensions.

In cancer detection, CNNs play a crucial role. These networks can analyze medical images and identify various patterns that indicate cancerous cells or damaged tissues. For example, in radiographic and mammographic images, CNNs can detect abnormal changes that may be signs of cancer. By training CNNs on large datasets of images from both cancerous and healthy samples, these networks learn to identify features associated with cancer cells and use new data for diagnosis.

Despite the impressive capabilities of CNNs in cancer detection, there are challenges as well. One of these challenges is the quality and diversity of data, as inappropriate data can lead to incorrect results. Additionally, accurate analysis and interpretation of results remain difficult due to the complexity of CNN structures, requiring specialized knowledge in both medical and artificial intelligence fields.

Overall, convolutional neural networks have become a powerful tool for detecting various types of cancers, contributing to significant advancements in the medical field, particularly in early cancer detection by improving accuracy and reducing diagnosis time.

II. METHODOLOGY

Criteria for Article Selection

To select the articles for this research, specific criteria were considered to provide a thorough and comprehensive review of the application of CNNs in cancer detection. One of our main criteria was the focus on using CNNs for cancer diagnosis, due to their efficiency and

capability in analyzing and interpreting medical images. This choice was driven by the power of CNNs in identifying and processing medical patterns, specifically related to cancer. Given the significant advancements in artificial intelligence in recent years and the improvements in the accuracy and speed of CNN-based diagnostics, articles published after 2020 were chosen as the time frame for inclusion. This allowed us to utilize the most up-to-date and reliable studies and explore newer methods in this field.

Data Collection Methods

For gathering the required articles, reputable scientific databases such as PubMed, IEEE, and other research platforms were used. These databases were selected because of their broad access and high-quality articles in the fields of artificial intelligence and medical research. Due to access restrictions to certain articles, we were constrained to those available for free or with open access. Although this limitation presented some challenges in article selection, the final collection of articles from these trusted sources was scientifically credible and reliable.

Timeframe and Scope of Reviewed Articles

From the approximately 20 articles initially selected and reviewed according to the above criteria, 10 top articles were ultimately chosen. These 10 articles not only specialized in cancer detection but also addressed various common and well-known types of cancer that are of significant clinical and medical importance. Given the fatal nature and diagnostic complexity of cancer, this selection allowed us to focus on research related to cancers analyzed using CNNs in a more detailed manner and examine the various aspects of each study.

General Objective and Evaluation Criteria in Article Review

The primary goal of this research is to provide a comprehensive review of CNN applications in cancer diagnosis, analyzing the architecture, accuracy, speed, and other effective aspects of these networks. In this regard, criteria such as CNN architecture type, diagnostic accuracy, processing speed, the datasets used, and the imaging techniques discussed in the articles were carefully examined. Additionally, the study aimed to explore how these networks function with different types of medical images (including radiology and MRI scans) and how they contribute to more precise and faster cancer predictions. Alongside these aspects, challenges and limitations related to implementing CNNs in this domain, such as the need for high computational power and access to diverse, high-quality datasets, were thoroughly analyzed.

Challenges and Limitations of the Research

During the article collection and selection process, we encountered various challenges. One of the primary challenges was the limited access to some significant articles in this field. Due to access restrictions, we were forced to use only freely available articles. Despite this limitation, efforts were made to select the most reliable articles in the field to ensure the research findings were credible and comprehensive.

The selected papers for this study, based on specific criteria, are presented in Table 2. These papers are a curated collection of relevant and reliable studies on the application of Convolutional Neural Networks in cancer detection.

III. Analysis and Comparison:

Prostate Cancer:

This study utilized the Harvard University MRI dataset, which includes 482 cases of prostate cancer and 200 cases of brachytherapy. The data was divided into two groups: 70% for training (478 images) and 30% for validation/testing (204 images). Using a CNN and Transfer Learning, the diagnostic process was simplified. Additionally, various methods such as Decision Tree and Support Vector Machine (SVM) were employed, with the best result achieved using the GoogLeNet model. In the GoogLeNet approach, the model achieved 100% accuracy. While other methods also produced satisfactory results, SVM achieved an accuracy of 99.71%. The initial losses of the model in the mini-batch (0.7086) and validation (0.4206) were reduced to near zero by iteration 30, and the validation accuracy reached 100% by iteration 45.¹⁵

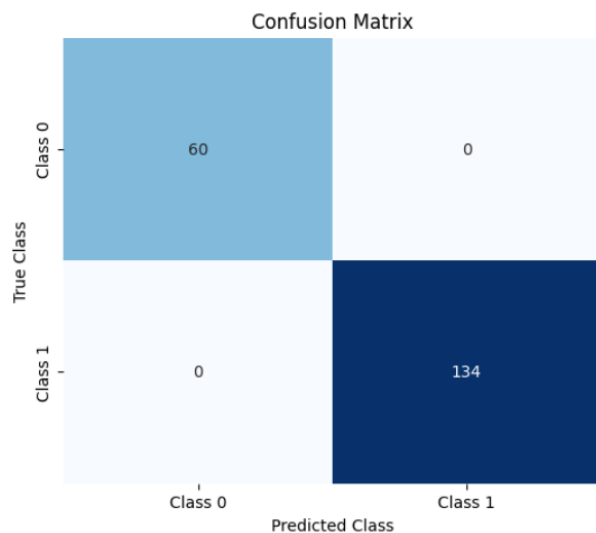


Fig6. Confusion matrix showcasing the performance of the CNN model in detecting prostate cancer, emphasizing its classification accuracy and false-positive rates.

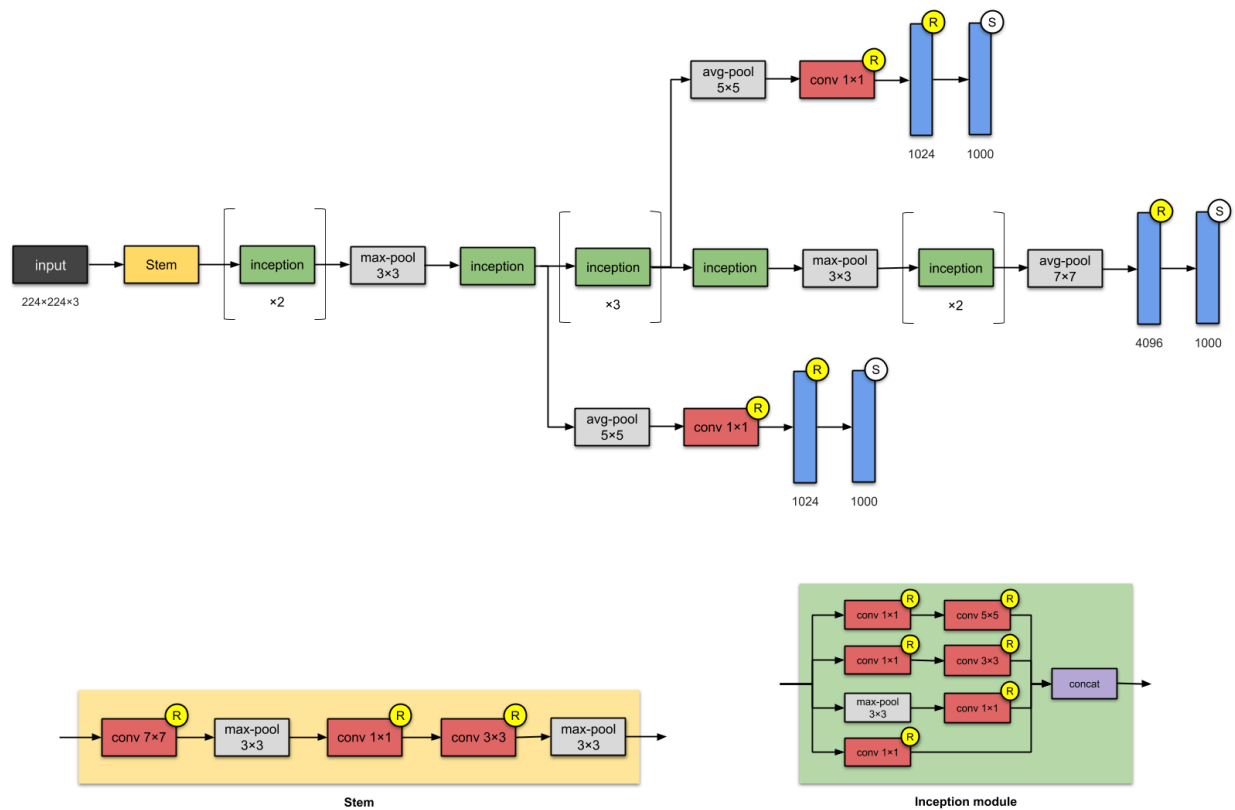


Fig7. Architectural illustration of the GoogLeNet model used in prostate cancer detection, detailing layers and connections.

Lung Cancer:

This study utilized the Iraqi Teaching Hospital Cancer Dataset (IQ-OTH/NCCD), which includes CT scans of patients with various types of lung cancer as well as some with healthy lungs. The dataset comprises 1,190 images categorized into three classes: benign, malignant, and normal. Unlike the previous study, this research employed the AlexNet model. A 70%-30% split was used for training and testing, respectively. After completing the training process, which was conducted randomly, the model achieved an overall accuracy of 93.548% after 86 out of 100 training epochs. Additionally, the model demonstrated a precision of 97.1015%, a sensitivity of 95.714%, and a specificity of 95%.¹⁶

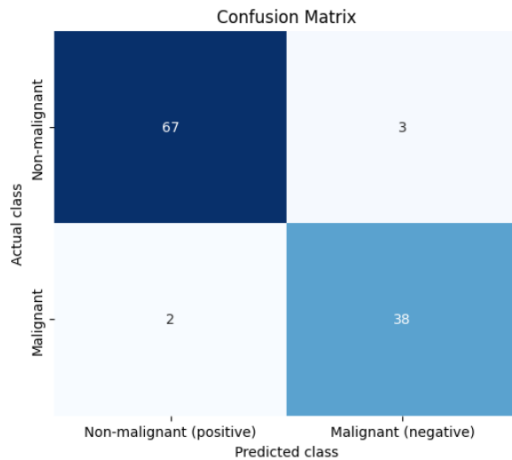


Fig8. Confusion matrix for the CNN model applied to lung cancer detection, highlighting precision, sensitivity, and specificity metrics.

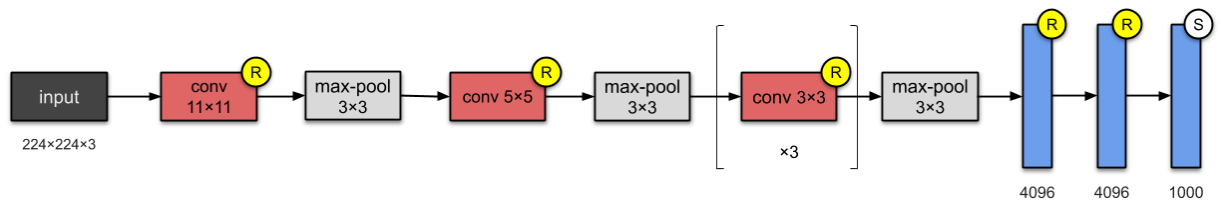


Fig9. Schematic representation of the AlexNet architecture, optimized for lung cancer classification, showing layers and kernel sizes.

Leukemia:

Unlike the previous two studies, this research did not use pre-trained models or Transfer Learning. Instead, it utilized a BCNN (customized convolutional neural network) architecture. The dataset included 260 microscopic images of cancerous and non-cancerous lymphocyte cells. The images were divided into two categories: cancerous and non-cancerous. For each category, 100 images were used for training, 15 for validation, and 15 for testing. The Hold-out method was applied for result validation.¹⁷

Several architectures were tested, differing in the number of convolutional layers and hidden layers. The best results were achieved with an architecture consisting of **3 convolutional layers** and **5 hidden layers**. The model's average accuracy was **94.00%** with a standard deviation of **2.00%**. Dropout rates were set at **20%** for convolutional layers and **50%** for fully connected layers to prevent overfitting. The models were trained using the **RMSprop optimizer** with a learning rate of **0.0001**, and the data was passed through the network 50 times during the

experimental phase. Dropout and other techniques were employed to further mitigate overfitting.¹⁷

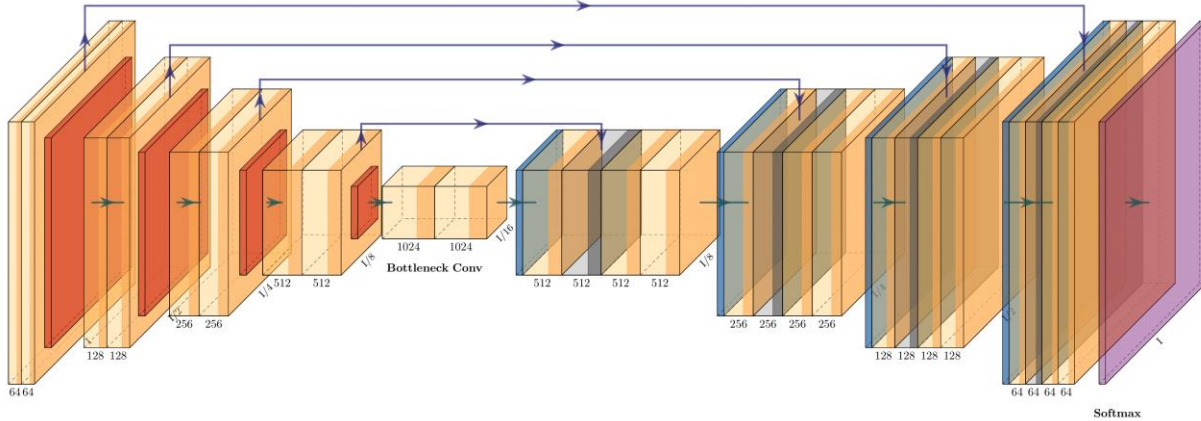


Fig10. Detailed architecture of the custom BCNN model used for leukemia diagnosis, illustrating its convolutional and fully connected layers

Bladder:

To train the model, GoogLeNet was first pre-trained using the ImageNet dataset, which includes 1.2 million publicly available images. This dataset contained 1,671 images of natural textures and 431 images of tumor lesions. Data preprocessing was minimal, and the images were electronically stored in TIFF format with a resolution of 1350×1080 pixels. Subsequently, it was further trained with 8,728 gastroscopy images to identify relevant texture features. Finally, transfer learning was applied using 2,102 cystoscopy images, including both normal and tumor samples, to optimize the model.¹⁸

The AI model's performance was evaluated by 53 observers at various experience levels and compared with pathological results and the Youden index. The CNN model, trained through a stepwise organic transfer learning approach, achieved a sensitivity of 95.4%, a specificity of 97.6%, an AUC of 0.98, and a Youden index of 0.930. Compared to various observers, including medical students and urologists, the AI model's diagnostic accuracy outperformed the observers' accuracy when tumors occupied more than 10% of the image. The model required only 5 seconds for diagnosis and 10 minutes for training.¹⁹

Skin:

Initially, we collected a dataset comprising 800 images of four types of skin cancer: actinic keratosis, basal cell carcinoma, malignant melanoma, and squamous cell carcinoma. Data augmentation techniques were then employed to increase the dataset size to 5,600 images. Subsequently, a deep CNN model was designed to train on this dataset. The model was trained using the Adam optimizer, a learning rate of 0.001, and the Cross-Entropy loss function. The proposed model achieved an accuracy of 95.98% on the test data, outperforming two pre-trained models (GoogLeNet and MobileNet). It showed a 1.76% higher accuracy compared to GoogLeNet and a 1.12% improvement over MobileNet, while remaining computationally comparable to other models.²⁰

In these studies, the InceptionV4 model, tested with classifiers such as SVM, Random Forest, and neural networks, achieved an accuracy of 89%, which was not satisfactory. Similarly, a modified ResNet-50 achieved an accuracy of 85.8% for single images and 86.6% for multimodal networks in classifying skin lesions, but it failed to achieve higher accuracy.

The GoogLeNet and MobileNet models, with 48 and 28 layers respectively, were pre-trained on the ImageNet dataset with 1,000 classes and demonstrated good performance. We used these models with their pre-trained weights, and our images had dimensions of 299×299. Additionally, we utilized the SGD optimizer and the Binary Cross-Entropy loss function.

Our proposed model achieved the highest accuracy of 97.23% in the Basal Cell Carcinoma (BCC) class, which also showed the highest precision, recall, and negative predictive values. To determine the best performance, we experimented with the SGD and Adam optimizers using MSE and Cross-Entropy loss functions. Employing the Adam optimizer with the Cross-Entropy loss function resulted in an accuracy of 95.98%, with precision and recall of 91.96% and 91.97%, respectively.

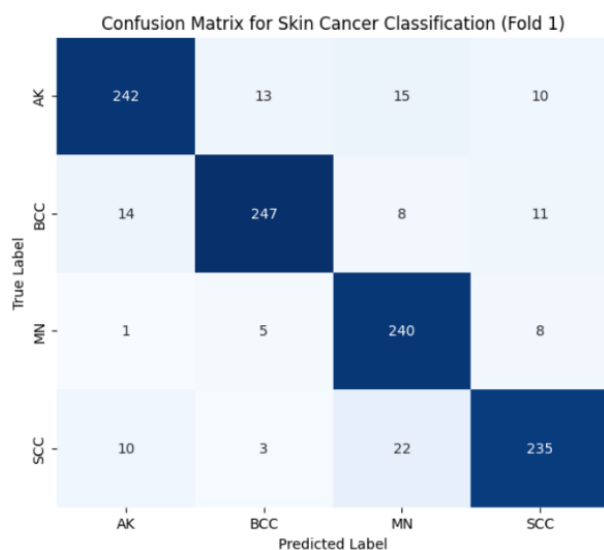


Fig13. Confusion matrix illustrating the CNN model's performance in detecting skin cancer, showcasing its accuracy and classification metrics.

Colorectal:

MRI images are utilized. The proposed model was compared with other existing CNN models such as VGG16, VGG19, Inception V3, Xception, GoogLeNet, ResNet50, ResNet100, and DenseNet. Based on experimental results, it was observed that VGG19 is the best deep learning approach for classifying colonoscopy images. Unlike most existing methods, the proposed model is fully automated and classifies images as benign, benign adenomatous, moderately differentiated malignant, and poorly differentiated malignant with an overall accuracy of 81% on 165 histopathological images.²¹

In general, medical images tend to have noise or quality reduction due to blurriness, which impacts the disease diagnosis process. One of the optimal filters used in image processing models is the Gaussian filter. Noise in the image can be smoothed by applying the Gaussian filter without introducing significant distortion.

The proposed model combines CNN and LSTM layers to enhance the ability to accurately identify tumor tissues and determine cancer stages from medical images. It employs an 18-layer CNN structure for feature extraction from pre-processed images, followed by a fully connected layer and a SoftMax function for multi-class classification.

The dataset comprises 334 images from patients with colorectal cancer, with 284 images used for training and 50 for testing. Data augmentation was applied to increase the dataset size fivefold. After seven iterations, the model achieved an accuracy of 94%.

With its 18-layer structure, the CNN achieved high sensitivity and accuracy, outperforming models such as ANN and BPNN. Its precision, recall, and accuracy were 92%, 93%, and 91%, respectively.

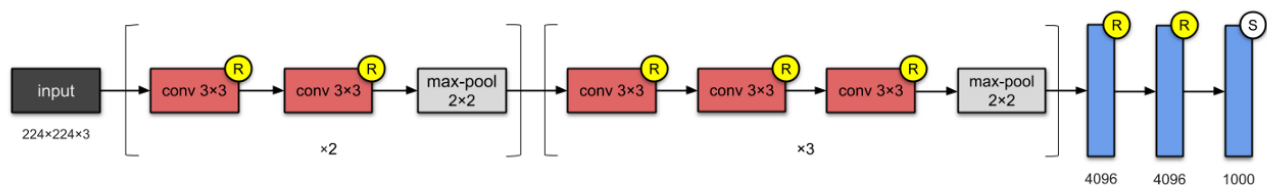


Fig 14. Architectural diagram of a CNN used for classifying colorectal cancer, highlighting key layers and connections

Liver:

This article introduces a model called ESP-UNet for liver segmentation in CT images, designed to prevent under-segmentation and over-segmentation. Additionally, liver cancer detection (ALCD) is performed using lightweight deep convolutional neural networks (DCNN).

The LiTS dataset, containing CT liver images, was used for this study, comprising 200 CT images (130 for training and 70 for testing).²²

The proposed methodology consists of three main stages:

1. **Enhancing** CT liver images using a modified dual-stage Gaussian filter (MDSGF).
2. **Segmenting** the liver region with UNet.
3. **Detecting** liver cancer using DCNN.

Abdominal CT images often have low contrast and blurriness, making liver segmentation challenging. The proposed MDSGF method improves image quality by combining a dual-stage Gaussian filter with CLAHE and mean filtering, enabling more accurate liver segmentation.

The input image is processed through two parallel UNet networks: The first UNet performs liver segmentation. The second UNet provides detailed edge information of the liver in the CT image.

By combining the outputs of these two UNets, issues of under-segmentation and over-segmentation are minimized.

The Kirsch filter, a nonlinear edge detector, identifies liver edges in CT images by calculating maximum edge strength in eight directions. This filter computes gradients with high precision and is less sensitive to noise.

UNet is a neural network for medical image segmentation comprising two main parts:

- **Compression:** Features are extracted using convolutional layers.
- **Expansion:** These features are used to reconstruct the image and enhance resolution.

The network is trained using optimization algorithms such as ADAM, SGDM, and RMSProp. The DCNN was tested with 2, 3, 4, and 5 layers, with the Adam optimizer yielding the best results.

The approach achieved accuracies of 87.10%, 92.90%, 95.70%, and 98.60% for 2-layer, 3-layer, 4-layer, and 5-layer DCNNs, respectively. The 5-layer DCNN was selected due to its fewer trainable parameters (437,000) compared to the 6-layer DCNN (889,000 parameters).

The 5-layer DCNN achieved remarkable results, delivering an accuracy of 98.60%, a precision of 0.97, a recall of 1.00, and an F1-score of 0.98. The training time for this model, using the LiTS dataset, was approximately 3,130 seconds.

The ESP-UNet model demonstrated superior performance in segmentation tasks, achieving a Dice score of 0.959 and a Jaccard index of 0.921. Similarly, the DCNN model achieved an impressive accuracy of 98.60%, with a recall of 1.00, a precision of 0.97, and an F1-score of 0.98.

Confusion Matrix

True Class	Predicted Class	
	Cancer	Normal
Cancer	35	1
Normal	0	34

Fig15. Confusion matrix presenting the CNN's results in liver cancer detection, emphasizing accuracy and recall rates.

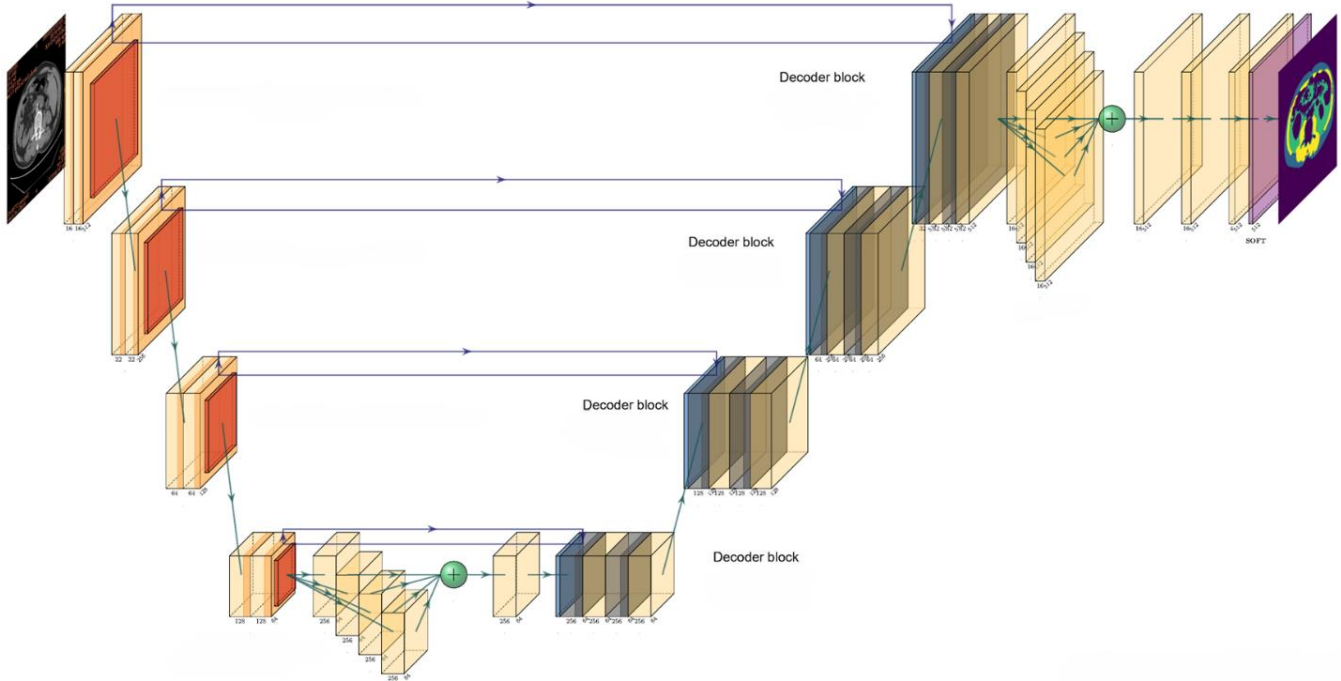


Fig16. Illustration of the ESP-UNet architecture used for liver cancer segmentation, including its compression and expansion pathways.

Breast:

This study utilized the DDSM database, which includes natural, malignant, and benign breast images, each category containing 650 images. Initially, the background of the images was removed, and Wiener filter and contrast-limited adaptive histogram equalization (CLAHE) were used for image reconstruction. To enhance image smoothness, wavelet packet decomposition (WPD) with the Daubechies wavelet (db3) at level 3 was applied.²³

For cancer detection, deep convolutional networks such as AlexNet and GoogLeNet were employed, and optimization algorithms like RMSprop, SGDM, and Adam were tested, each with different learning rates.

In this method:

1. **Preprocessing:** DDSM images were converted to binary images, breast tissue and muscle intensity were enhanced, and unnecessary information was removed. The background was discarded by eliminating zero-intensity pixels, and the image was refined using Otsu's grayscale thresholding method. Noise was reduced using the Wiener filter and signal-to-noise ratio (SNR) adjustment to enhance image quality.
 - **Wiener filter:** Used to remove noise and reconstruct image blurriness by leveraging the spectral power of the image and noise.
 - **CLAHE filter:** Enhanced image contrast by locally adjusting the histogram.
2. **Wavelet Packet Decomposition (WPD):** Used to eliminate non-stationary noise while preserving edges and texture by decomposing the image into sub-images across different directions.

These combined techniques improved the quality and clarity of breast cancer images.

The DDSM images were randomly divided into 70% for training and 30% for testing. Training was conducted using learning rates of 0.01, 0.001, and 0.0001 with SGDM, Adam, and RMSprop as optimizers.

The networks used for breast cancer image detection include GoogLeNet, AlexNet, Multi-Layer Perceptron (MLP), and MLP optimized with PSO and ACO algorithms (PSO-MLP and ACO-MLP). The accuracy and loss function values for GoogLeNet and AlexNet were evaluated with a learning rate of 0.001. GoogLeNet achieved an accuracy of 98.23% in the first epoch with the Adam optimizer, after which fluctuations and error rates decreased. Both GoogLeNet and AlexNet demonstrated low error values by around the 50th iteration when using Adam as the optimizer.

Performance Results:

GoogLeNet Achieved the best performance in terms of accuracy and runtime, with an accuracy of 99% and a runtime of 4.14 minutes. AlexNet achieved an accuracy of 98.91% but had a longer runtime of 4.71 minutes. PSO-MLP and ACO-MLP were 90.21% and 86.14% accurate respectively.

Ovarian:

For identifying ovarian cancer in transgenic mice, Optical Coherence Tomography (OCT) imaging recordings were utilized. Classification was performed using a neural network capable of understanding ordered spatial topographical sequences. Three neural network-based approaches were proposed:

1. **A VGG-supported feedforward network.**
2. **A 3D Convolutional Neural Network (3D CNN).**
3. **A Convolutional Long Short-Term Memory (ConvLSTM) network.**

These methods can automatically identify significant features without requiring manual feature extraction.²⁴

The comparison of the models shows the following:

- The **VGG model** has the highest number of learned parameters (**23,121,729**) but requires the least training time (**201ms per sample**).
- The **ConvLSTM model** has the longest training time (**700ms per sample**).
- The **3D CNN model** has the lowest number of parameters (**1,140,477**) and moderate training time (**417ms per sample**).

Challenges:

One issue in using OCT for ovarian cancer screening is the presence of optical noise and the 3D nature of the data, which involves challenges of scaling and depth dependency in imaging performance. Unlike previous studies, this research used images of mice for training, adding a unique aspect to the approach.

Data Collection:

- **Imaging System:** OCS1050SS, contactless mode.
- **Wavelength:** 1040 nm.
- **Lateral and axial resolution:** 11 μm , 1 μm .
- **Imaging volume:** 4 mm width and 2 mm depth.
- **Digital image dimensions:** 750 \times 752 \times 512 pixels.

In the preprocessing stage, the pixel values were scaled to the range of $[-1, 1]$. A Gaussian filter was applied to reduce noise in the images, enhancing their overall quality. Additionally, standardization was performed to further improve the data quality, ensuring better consistency and reliability for the subsequent analysis.

The **VGG model** used transfer learning, initialized with pre-trained weights on the ImageNet dataset, and fine-tuned with the OCT data. L2 regularization was employed to normalize weights in the encoder-decoder layers, and dropout was applied.

In contrast, the **ConvLSTM model** did not use normalization or dropout. Cross-entropy loss was used for optimization.

Performance:

The results indicated the following Area Under the Curve (AUC) values:

1. **VGG model:** Peak AUC = 0.86, Mean AUC = 0.59.
2. **ConvLSTM model:** Peak AUC = 0.98, Mean AUC = 0.81.
3. **3D CNN model:** Peak AUC = 0.92, Mean AUC = 0.69.

The **ConvLSTM model** demonstrated the best performance with a **Peak AUC of 0.98**, outperforming the **3D CNN model (Peak AUC = 0.92)** and the **VGG model (Peak AUC = 0.86)**.

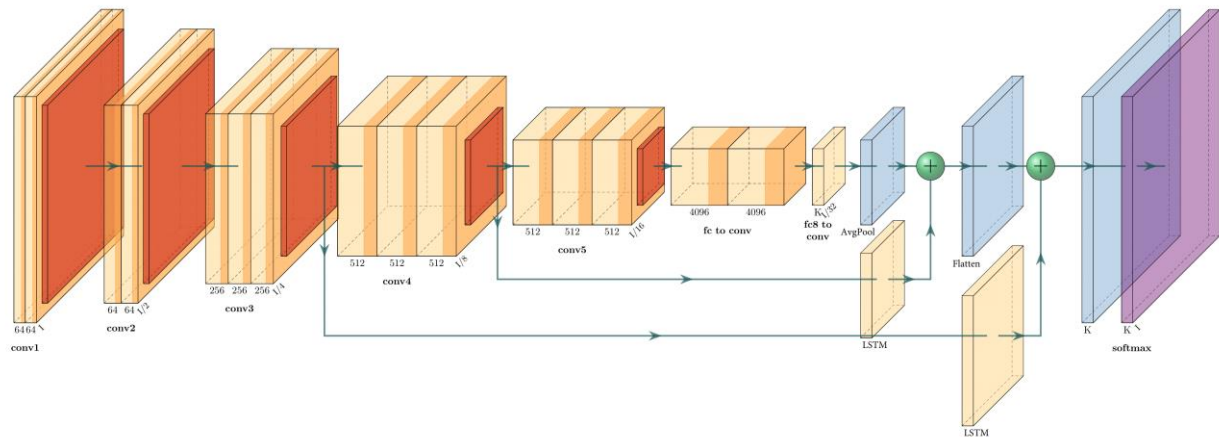


Fig18. Architecture diagram of the model used for ovarian cancer detection, showcasing its feature extraction capabilities.

Thyroid:

This study is the first to utilize **Xception**, a state-of-the-art Convolutional Neural Network (CNN), for thyroid cancer detection. The **Xception model** was compared to other models

The **MXTCD framework** used in this study consists of two stages:

1. **Stage 1:** Medical images are fed into the Xception model for binary classification. This stage evaluates the impact of the type of medical images (CT and ultrasound) on diagnostic results, with model tuning applied to different datasets.
2. **Stage 2:** Multi-channel architectures based on Xception are applied for binary and multi-class classification tasks tailored to the needs of clinicians. Three optional architectures were proposed:
 - **SIDC (Single Input Dual Channel):** Combines input channels into a unified model.
 - **DIDC (Dual Input Dual Channel):** Combines dual inputs for more refined classification.
 - **Four-Channel Architecture:** Processes four input channels simultaneously for high accuracy.

Xception, inspired by the Inception model, uses depth wise separable convolutions to extract spatial and channel-wise correlations. It outperformed other models such as VGG16 and ResNet152 in both accuracy and execution time in the ImageNet competition.

The dataset includes 448 DDTI ultrasound images (66 benign and 382 malignant), 917 Hospital_X ultrasound images (200 benign and 717 malignant), and 2352 Hospital_X CT scan images (578 benign and 514 malignant after removing 577 non-diagnostic images). The ultrasound images were labeled based on TIRADS scores, and the CT scans were labeled based on histopathological results. The images were cropped and labeled using a Python-based thyroid segmentation tool, and all images were resized to 224×224 pixels.²⁵

Performance:

Xception performed better than all other models:

1. **Ultrasound DDTI:** Accuracy = **0.980**.
2. **Hospital_X Ultrasound:** Accuracy = **0.987**.
3. **CT scans (Left Side):** Accuracy = **0.966**.
4. **CT scans (Right Side):** Accuracy = **0.970**.

Additionally, Xception achieved high scores in **predictive accuracy**, **NPV (Negative Predictive Value)**, **recall**, and **F1 score**. Although ResNet10 had the fastest execution time, Xception and DenseNet121 showed comparable execution speeds.

In this study, the results of multi-channel architectures were analyzed with a focus on optimizing filter sizes for SIDC. Filter sizes of 3×3 and 7×7 were tested, with the 7×7 filter providing better accuracy. Specifically, the accuracy for DDTI ultrasound reached 0.984, Hospital_X ultrasound reached 0.988, left CT scans achieved 0.972, and right CT scans reached 0.974. Compared to other models, SIDC showed slight improvements across all datasets. For example, the accuracy for DDTI ultrasound increased from 0.984 to 0.987 with SIDC. Additionally, when comparing DDC and the four-channel model, DDC had an average accuracy of 0.95, while the four-channel model achieved 0.94. The four-channel model performed better for "normal" patients (accuracy = 1.00), while DDC outperformed in "abnormal" cases.

A comparison with previous studies revealed that prior research using ultrasound reported diagnostic accuracies between 70% and 92%, whereas this study achieved DDTI ultrasound accuracy of 0.980 and Hospital_X ultrasound accuracy of 0.987. For CT scans, existing studies reported accuracies ranging from 90.4% to 95.73%, while this study achieved 0.966 for left CT and 0.970 for right CT. Furthermore, using the SIDC architecture, accuracy for both sides improved to 0.975.

The results indicate that the Xception model and its multi-channel architectures outperformed single-channel CNN models and demonstrated superior performance compared to other studies in thyroid cancer detection, particularly when incorporating CT scans.²⁵

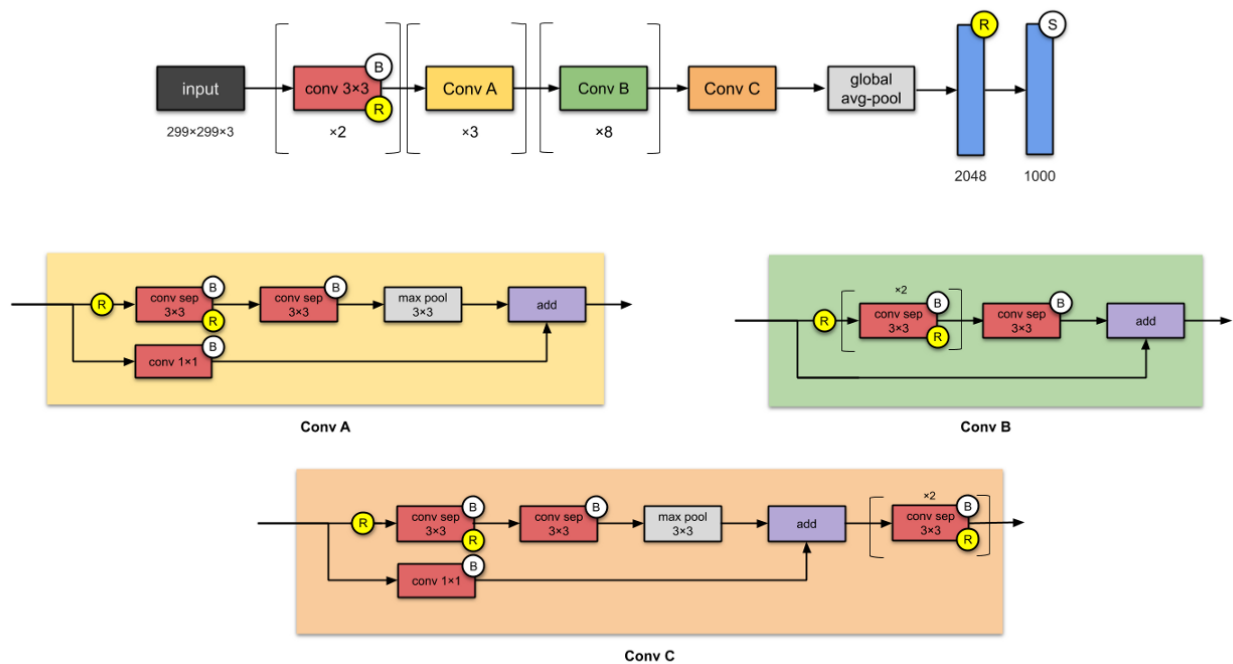


Fig19. Architectural representation of the Xception model optimized for thyroid cancer detection, highlighting its depth wise separable convolutions and multi-channel architecture

Cancer Type	Dataset Used	Imaging Technique	CNN Architecture	Accuracy (%)	Loss Function	Optimizer
Breast	DDSM	Mammography, Ultrasound	AlexNet, GoogLeNet	99.0	Binary Cross entropy	SGDM, RMSprop, Adam
Lung	IQ-OTH/NCDD	CT scans	AlexNet	93.54	Binary Cross entropy	Adam
Colorectal	TCGA-CRC-DX	Histopathology	VGG19	92.0	Cross entropy	Adam, SVM classifier
Thyroid	DDTI, CT Hospital_X	Ultrasound	Xception	97.5	Dice Loss	Adam
Ovarian	OVCAD	OCT	VGG16-LSTM Hybrid	98.0	Mean Squared Error (MSE)	SGD
Liver	LiTS	CT scans	U-Net	98.6	Binary Cross entropy	Adam
Bladder	Custom Dataset	Cystoscopy	GoogLeNet	98.0	Cross entropy	Adam
Blood	ALL-IDB, C-NMC	Microscopy Images	BCNN-LSTM Hybrid	94.0	Binary Cross entropy	RMSprop
Prostate	PROMISE12	MRI	GoogLeNet, SVM	100	Binary Cross entropy	Adam
Melanoma	ISIC	Dermoscopy Images	Custom, MobileNet, GoogleNet	95.98	Binary Cross entropy	Adam

Table 2. Comprehensive comparison of the articles reviewed above, highlighting the key aspects of each CNN mode.

IV. **Conclusion:**

This study confirms that Convolutional Neural Networks (CNNs), as one of the most advanced methods for analyzing medical images, have played a vital role in diagnosing various types of cancer. The reviews indicate that these models provide remarkable diagnostic accuracy, often exceeding 95% and reaching up to 99% in certain cases. For instance, the GoogLeNet model achieved 99% accuracy with a runtime of 4.14 minutes for breast cancer detection, while AlexNet showed slightly lower performance with 98.91% accuracy and a longer runtime of 4.71 minutes.

In thyroid cancer, the Xception model achieved accuracy ranging from 96.6% to 98.7%, depending on the type of data (ultrasound or CT scans). For ovarian cancer, ConvLSTM demonstrated superior performance with 98% accuracy and an AUC of 0.98, compared to models like VGG, which recorded an AUC of 0.86. In skin cancer, a custom CNN model utilizing augmented data achieved 95.98% accuracy, outperforming GoogLeNet and MobileNet, which had accuracies of 94.22% and 94.86%, respectively.

Regarding data limitations, in prostate cancer with only 600 samples, the GoogLeNet model achieved 99.71% accuracy through transfer learning. For liver cancer, the ESP-UNet model provided 98.6% accuracy in identifying cancerous regions from CT scans. This study also showed that preprocessing methods, such as Gaussian filters, CLAHE techniques, and wavelet decomposition, effectively reduced noise and enhanced data quality.

Challenges, such as the scarcity of human data in some studies—particularly ovarian cancer where data was collected from mice—created limitations. However, techniques like data augmentation and transfer learning have effectively mitigated these issues. Furthermore, the use of methods such as dropout and L2 regularization successfully prevented overfitting, increased model accuracy, and reduced errors.

Ultimately, this research demonstrates that with the expansion of datasets, improved preprocessing techniques, and the utilization of more advanced CNN architectures, higher accuracy and faster diagnostics can be achieved. CNN technology holds significant potential to become a key tool in clinical systems, aiding in reducing the cost and time of cancer diagnosis in the future.

References:

- 1 Mattiuzzi, C. & Lippi, G. Current cancer epidemiology. *Journal of epidemiology and global health* **9**, 217-222 (2019).
- 2 Sung, H. *et al.* Global cancer statistics 2020: GLOBOCAN estimates of incidence and mortality worldwide for 36 cancers in 185 countries. *CA: a cancer journal for clinicians* **71**, 209-249 (2021).
- 3 Bai, J.-W., Qiu, S.-Q. & Zhang, G.-J. Molecular and functional imaging in cancer-targeted therapy: current applications and future directions. *Signal Transduction and Targeted Therapy* **8**, 89 (2023).
- 4 Gandaglia, G. *et al.* Epidemiology and prevention of prostate cancer. *European urology oncology* **4**, 877-892 (2021).
- 5 Saginala, K. *et al.* Epidemiology of bladder cancer. *Medical sciences* **8**, 15 (2020).
- 6 Morgan, E. *et al.* Global burden of colorectal cancer in 2020 and 2040: incidence and mortality estimates from GLOBOCAN. *Gut* **72**, 338-344 (2023).
- 7 Chen, J.-G. *et al.* Liver cancer mortality over six decades in an epidemic area: what we have learned. *PeerJ* **9**, e10600 (2021).
- 8 Lei, S. *et al.* Global patterns of breast cancer incidence and mortality: A population-based cancer registry data analysis from 2000 to 2020. *Cancer Communications* **41**, 1183-1194 (2021).
- 9 Huang, J. *et al.* Worldwide burden, risk factors, and temporal trends of ovarian cancer: a global study. *Cancers* **14**, 2230 (2022).
- 10 Huang, J. *et al.* Distribution, risk factors, and temporal trends for lung cancer incidence and mortality: a global analysis. *Chest* **161**, 1101-1111 (2022).
- 11 Alzubaidi, L. *et al.* Review of deep learning: concepts, CNN architectures, challenges, applications, future directions. *Journal of big Data* **8**, 1-74 (2021).
- 12 Barbu, A., Lu, L., Roth, H., Seff, A. & Summers, R. M. An analysis of robust cost functions for CNN in computer-aided diagnosis. *Computer Methods in Biomechanics and Biomedical Engineering: Imaging & Visualization* **6**, 253-258 (2018).
- 13 Cui, N. in *Journal of Physics: Conference Series*. 012027 (IOP Publishing).
- 14 Bhatt, D. *et al.* CNN variants for computer vision: History, architecture, application, challenges and future scope. *Electronics* **10**, 2470 (2021).
- 15 Abbasi, A. A. *et al.* Detecting prostate cancer using deep learning convolution neural network with transfer learning approach. *Cogn Neurodyn* **14**, 523-533 (2020).
<https://doi.org/10.1007/s11571-020-09587-5>
- 16 Huang, J. *et al.* Distribution, Risk Factors, and Temporal Trends for Lung Cancer Incidence and Mortality: A Global Analysis. *Chest* **161**, 1101-1111 (2022).
<https://doi.org/10.1016/j.chest.2021.12.655>
- 17 Billah, M. E. & Javed, F. Bayesian Convolutional Neural Network-based Models for Diagnosis of Blood Cancer. *Applied Artificial Intelligence* **36** (2021).
<https://doi.org/10.1080/08839514.2021.2011688>
- 18 Saginala, K. *et al.* Epidemiology of Bladder Cancer. *Med Sci (Basel)* **8** (2020).
<https://doi.org/10.3390/medsci8010015>

- 19 Ikeda, A. *et al.* Cystoscopic Imaging for Bladder Cancer Detection Based on Stepwise Organic Transfer Learning with a Pretrained Convolutional Neural Network. *J Endourol* **35**, 1030-1035 (2021). <https://doi.org/10.1089/end.2020.0919>
- 20 Junayed, M. S., Anjum, N., Sakib, A. & Islam, M. B. in *Computer Science Research Notes* (2021).
- 21 Karthikeyan, A., Jothilakshmi, S. & Suthir, S. Colorectal cancer detection based on convolutional neural networks (CNN) and ranking algorithm. *Measurement: Sensors* **31** (2024). <https://doi.org/10.1016/j.measen.2023.100976>
- 22 Napte, K. M., Mahajan, A. & Urooj, S. Automatic Liver Cancer Detection Using Deep Convolution Neural Network. *IEEE Access* **11**, 94852-94862 (2023). <https://doi.org/10.1109/access.2023.3307640>
- 23 Rajakumari, R. & Kalaivani, L. Breast Cancer Detection and Classification Using Deep CNN Techniques. *Intelligent Automation & Soft Computing* **32**, 1089-1107 (2022). <https://doi.org/10.32604/iasc.2022.020178>
- 24 Schwartz, D., Sawyer, T. W., Thurston, N., Barton, J. & Ditzler, G. Ovarian cancer detection using optical coherence tomography and convolutional neural networks. *Neural Comput Appl* **34**, 8977-8987 (2022). <https://doi.org/10.1007/s00521-022-06920-3>
- 25 Zhang, X., Lee, V. C. S., Rong, J., Liu, F. & Kong, H. Multi-channel convolutional neural network architectures for thyroid cancer detection. *PLoS One* **17**, e0262128 (2022). <https://doi.org/10.1371/journal.pone.0262128>